Polymer 51 (2010) 4880–4890

Contents lists available at ScienceDirect

Polymer

journal homepage: www.elsevier.com/locate/polymer

The toughening mechanism in hybrid epoxy-silica-rubber nanocomposites (HESRNs)

Y.L. Liang, R.A. Pearson*

Center for Polymer Science and Engineering, Lehigh University, 5 East Packer Ave, Bethlehem, PA 18015-3195, USA

ARTICLE INFO

Article history:
Received 29 November 2009
Received in revised form
24 August 2010
Accepted 25 August 2010
Available online 15 September 2010

Keywords:
Hybrid nanocomposites
Nanosilica
Toughening mechanism

ABSTRACT

Two different size nanosilica (NS) particles, nominally 20 nm and 80 nm in diameter, and carboxyl terminated butadiene acrylonitrile (CTBN) were blended into a lightly crosslinked, DGEBA/piperidine epoxy system to investigate the toughening mechanisms in hybrid epoxy-silica-rubber nanocomposites (HESRNs). Adding small amount of NS particles into CTBN toughened epoxies further improved the fracture toughness to a level that could not be achieved by increasing CTBN content alone. Interestingly, this toughening effect is diminished when NS particles clustered at high CTBN contents. In addition, the effect of NS particle size on toughening behavior was not considerable, except the case when NS clustering is observed. According to the SEM and TOM investigations, the plastic zone, which consists of shear banding and matrix dilation, is further enlarged in front of the crack tip in HESRNs. Irwin's model is used to evaluate the process zone concept and the result indicates that zone shielding is credited for the toughening mechanism in these HESRNs.

1. Introduction

Epoxy toughening agents can be categorized into three types: soft rubber particles, rigid inorganic fillers and semi-rigid organic fillers. Substantial differences in mechanical properties and toughening mechanisms have been reported for these three types of toughening agents [1–14]. Generally speaking, rubber particles toughened epoxies usually demonstrate superior fracture toughness but result in a decrease in stiffness and strength when compared to the epoxies toughened by the other two types of toughening agents [7–14]. In addition, many studies have reported a peak or plateau in fracture toughness when rubber particles are used.

One way to further enhance the fracture toughness of epoxies is to take advantage of different toughening mechanisms, i.e. soft particles and rigid fillers can be simultaneously mixed into epoxy resins to enhance fracture toughness. For example, hybrid epoxy composites consisting of rubber particles and micron-size glass spheres have been shown to possess a synergistic toughening effect [15–18] and improved fatigue crack propagation (FCP) resistance [19,20].

Recently, nanometer size silica has been introduced to rubber toughened epoxies with considerable improvements in fracture toughness [21–26]. It is interesting to note that the toughening mechanisms in these hybrid nanocomposites are not yet clearly understood. In order to further understand the fracture behavior of hybrid nanocomposites, a brief review of the toughening mechanisms in modified and/or filled epoxies is given below.

1.1. Toughening mechanisms in rubber toughened epoxies

For rubber toughened epoxies, increased fracture toughness results from the rubber particle cavitation, concomitant matrix shear banding and plastic matrix dilation [1–6]. Specifically, matrix shear banding and matrix dilation form a plastic zone in front of crack tip, which shields the crack tip from the applied crack driving force and blunts crack propagation [2,5]. Rubber particle cavitation contributes very little to the overall toughness directly but indirectly rubber particle cavitation enables matrix dilation and shear banding [4,5]. Huang and Kinloch [2,3] have proposed a toughening model that attempts to quantify the contributions of three distinct micromechanisms to the overall fracture toughness. In their model, rubber particle bridging contributes the least to the overall fracture toughness hence matrix shear banding and matrix plastic dilation are the micromechanisms credited for more than 90% contribution of fracture energy enhancements at room temperature.

1.2. Toughening mechanisms in glass sphere toughened epoxies

Numerous toughening mechanisms have been proposed for micron-size glass spheres filled epoxies. Crack front pinning [7], particle bridging [8], crack-path deflection [9,10], and matrix microcracking [11] are among those mechanisms reported in

* Corresponding author. Tel.: +1 610 758 3857; fax: +1 610 758 4244.
E-mail address: rp02@lehigh.edu (R.A. Pearson).

0032-3861/$ – see front matter © 2010 Published by Elsevier Ltd.
doi:10.1016/j.polymer.2010.08.052

literature. Such mechanisms have been modeled and verified with experimental data. It is noteworthy that there is somewhat of a controversy in regards of particle size effect between some traditional toughening models and the nanocomposites studies. In fact, crack front pinning, filler bridging, and crack-path deflection models all predict that larger diameter fillers (in micron range) are more efficient for toughening purposes [7–9], but recent studies have observed that much smaller nanometer size rigid spheres can significantly increase the fracture toughness of nanocomposites [27–31]. Parenthetic speaking, our current work has further demonstrated that nanometer size silica spheres play a similar role as rubber particles in toughening epoxy [31].

1.3. Toughening mechanisms in hybrid epoxy-silica-rubber composites

There is no exclusive interpretation of toughening mechanisms in hybrid epoxy-silica-rubber composites due to the complicated compositions and the interactions between various toughening agents. It is generally accepted that the matrix shear banding as well as the matrix dilation seen in the hybrid composites are due to the addition of rubber particles [15–20]. On the other hand, many studies credited the toughening effect of adding micron-size glass spheres into the hybrid composites to the crack pinning mechanism. For example, Kinloch at al [15], Maazouz et al. [16], and Zhang et al. [17] individually observed the crack front bowing and characteristic tails on the fracture surfaces, which are considered as the crack pinning mechanism patterns, from their hybrid composite systems.

In regards of the synergistic interaction in hybrid composites, more interpretations can be found in the following studies [19,20]. Azimi and his coworkers demonstrated a synergistic toughening effect in static fracture toughness as well as the fatigue crack propagation (FCP) resistance when blending micron-size glass spheres (49 μm in diameter) into the rubber toughened epoxy resins. After carefully investigating the fracture surfaces and subsurfaces, they attributed the synergistic improvement to the further enhanced crack pinning mechanism induced by the rubber particle cavitation [19]. More specific speaking, rubber particle cavitation releases tri-axial stress and suppresses the debonding between glass spheres and matrix. The suppressed debonding magnifies the crack pinning mechanism and further enhances the fracture toughness of the hybrid composites. Azimi et al. [20] also reported that the addition of the hollow glass spheres (HGS) into rubber toughened epoxies results a similar synergistic toughening effect in both static fracture toughness and FCP resistance. They elucidated that this synergistic toughening effect results from an interaction between the stress fields of the crack tip process zone and the HGS in this particular hybrid composite system. Interestingly, this interaction facilitates plastic zone branching which induces further improvement in fracture toughness. Additionally, Lee and Yee [18] pointed out the presence of micron-size glass spheres can enhance the rubber cavitation/shear yielding mechanism, since the process zone length in hybrid composites is further increased compared with the rubber toughened epoxy.

1.4. Hybrid epoxy-silica-rubber nanocomposites

Despite the fact that the size of nanosilica (NS) particles are considered too small to provide crack pinning or crack deflection effect [28], investigators recently showed that blending NS particles into rubber toughened epoxy systems further enhanced the fracture energy of the hybrid epoxy-rubber-silica nanocomposites (HESRNs) [21–23]. The toughening behavior varies in different HESRN systems. For example, it has been reported that adding small amounts of NS particles causes significant increase in fracture energy for a room temperature cured, amine terminated butadiene acrylonitrile (ATBN) toughened epoxy [21,22]. The fracture energies of these particular HESRNs demonstrate a maximum peak when 5 wt.% NS was applied. A dissimilar toughening behavior was also reported by the same research group. Kinloch et al. [23] blended NS particles to a carboxyl terminated butadiene acrylonitrile (CTBN) toughened, high temperature cured epoxy/anhydride system, and showed the increase in fracture energy was proportional to NS content up to 15.4 wt.% without any maximum peak. It appears that the toughening behavior in HESRNs can be influenced by the different curing agents used as well as the different types of rubber modifier.

To summarize the literature review, it is obvious that the toughening mechanisms proposed for micron-size silica cannot be used to explain the improvements of fracture behavior in hybrid epoxy-silica-rubber nanocomposites (HESRNs) since NS particles are not large enough to offer such toughening effects according to crack pinning, particle bridging, and crack deflection mechanisms. Recent studies have showed substantial toughness improvements in HESRNs, but the elucidation of the toughening mechanisms remains incomplete. In this study, the effect of NS size and the NS dispersion status on the toughening behavior in HESRNs will be presented. Additionally, the toughening mechanisms in HESRNs will also be discussed.

2. Experimental approach

2.1. Materials

Two different size nanosilica (NS) particles, nominally 20 nm and 80 nm in diameter were applied in this study. 20 nm (Nanopox E430, Nanoresins) and 80 nm (3M) NS particles were pre-dispersed in di-glycidyl ether of bisphenol A/F (DGEBA/F), and DGEBA epoxy resin as received, respectively. Both NS particles were supplied as concentrated dispersions, therefore, a DGEBA epoxy resin (DER331, Dow Chemical, Co.) was used to adjust the NS fraction from 1.25 wt.% to 25 wt.%. A conventional reactive liquid rubber, carboxyl terminated butadiene acrylonitrile copolymer, (CTBN Hycar®1300x8, Emerald Performance Materials) was chosen as the rubber modifier. After 4 h mixing, 5 phr (parts per hundred parts resin) curing agent (piperidine, Aldrich) was added, and the studied materials were cured at 160 °C for 6 h.

In order to investigate the effect of NS content on toughening effect, the CTBN was kept constant as 18 wt.% in the first part of this study. More details including the designations of each formulation in these HESRNs (I–V) with fixed CTBN contents can be found in Table 1. For the second part of this study, the CTBN content was varied and the NS content was fixed at 5 wt.% (see Table 2). The epoxy-rubber blends (ERBs) with similar amounts of CTBN were tested to provide comparative benchmarks (see Table 3).

It is noteworthy to mention that the volume fractions of the ingredients were determining using the weight ratio of each

Table 1
Formulations for HESRNs (I–V) with constant CTBN content (18 wt.%).

Designation	I	II	III	IV	V
Rubber (g)	27	27	27	27	27
NS (g)	1.9	3.8	7.5	15.0	37.5
Total Epoxy (g)	115.8	113.6	110.0	102.5	81.3
Piperidine (g)	5.8	5.7	5.5	5.1	4.1
Summary (g)	150.5	150.1	150.0	149.6	149.9
NS (wt.%)	1.25%	2.50%	5.00%	10.03%	25.03%
Rubber (wt.%)	18%	18%	18%	18%	18%
NS (vol%)	0.8%	1.5%	3.1%	6.4%	16.8%
Rubber (vol%)	20.6%	20.7%	20.9%	21.3%	22.6%

Table 2
Formulations for HESRNs (A–E) with constant NS content (5 wt.%).

Designation	A	B	C	D	E
Rubber (g)	4.5	7.5	15	21	27
NS (g)	7.5	7.5	7.5	7.5	7.5
Total Epoxy (g)	131.8	129.3	121.3	115.3	110.3
Piperidine (g)	6.6	6.5	6.1	6.8	5.5
Summary (g)	150.3	150.7	149.8	150.5	150.3
NS (wt.%)	5.0%	5.0%	5.0%	5.0%	5.0%
Rubber (wt.%)	3%	5%	10%	14%	18%
NS (vol%)	3.2%	3.2%	3.2%	3.1%	3.1%
Rubber (vol%)	3.7%	6.0%	12.0%	16.6%	20.9%

component and the in corresponding densities given by the manufacturers or references as following. NS: 1.8 g/cm^3 [28]; Epoxy: 1.16 g/cm^3; CTBN: 0.948 g/cm^3, and piperidine: 0.86 g/cm^3. Other details in regards to the sample preparation and curing process can be found in our previous study [31].

2.2. Experimental methods

For the NS particle dispersion study, the composite samples were sent to Core Electron Microscopy Facility in UMass Medical School for transmission electron microscopy (TEM) investigation. The TEM samples were cryo-microtomed into 80–120 nm thin sections under −10 °C. Later on, some of the samples were stained with osmium tetroxide (OsO_4) and then supported on gold (Au) grids for TEM examination. The electron-dense OsO_4 adds to the carbon–carbon double bonds of the CTBN and is able to enhance the contrast due to its large scattering cross-section [5].

The glass transition temperatures, T_g, of cured epoxies were determined using the mid-point of the glass transition process according to the second scan from differential scanning calorimeter (DSC, model 2920, TA Instrument). The sample weight ranged from 10 to 20 mg and the heating rate was 10 °C/min.

A screw-driven materials testing machine (model 5567, Instron) was used to characterize the mechanical properties of the studied materials under ambient temperature. Compression tests were conducted by following ASTM D695 [32] guidelines with tetragonal shaped specimens of 5.0 mm × 5.0 mm × 10.0 mm. The cross-head speed was 1 mm/min. At least 5 samples for each formulation were tested. The compressive modulus and the yield stress were recorded for the calculation of the fracture energy and the estimation of plastic zone size. Note that the compressive modulus is used to approximate the tensile modulus, i.e. Young's modulus.

Fracture toughness, K_{IC}, was measured according to ASTM D5045–99 guidelines under monotonic loading conditions [33]. A single-edge-notched, three point-bending (SEN-3PB) specimen was chosen with the following dimensions: 76.2 mm × 12.7 mm × 6.4 mm. At least 5 samples for each formulation were tested. Fracture energy, G_{IC}, was calculated using Eq. (1) [33]. Where E is Young's modulus, which was assumed to equal the compression modulus in this study. The Poisson's ratio, ν, is taken as 0.39 for the epoxy system [34].

Table 3
Formulations of epoxy-rubber blends (ERBs).

ERBs/CTBN	A	B	C	D	E
CTBN (g)	4.5	7.5	15	21	27
Total Epoxy (g)	138.6	135.7	128.5	123.0	117.1
Piperidine (g)	6.6	6.5	6.8	6.5	6.2
Summary (g)	149.7	149.7	150.3	150.5	150.3
CTBN (wt.%)	3%	5%	10%	14%	18%
CTBN (vol%)	3.6%	6.0%	11.8%	16.4%	20.9%

$$G_{IC} = \frac{K_{IC}^2(1-\nu^2)}{E} \quad (1)$$

A scanning electron microscopy (SEM, model 4300, Hitachi) was used for fracture surface studies. Before the SEM investigation, the fractured surfaces from the 3PB specimens were coated with Iridium as the electrically conductive layer through sputter coating (turbo putter coater, model EMS575X, Electron Microscopy Sciences). The coating condition was chosen as following to maintain the 5 nm thick Iridium layer: coating current 20 mA, coating time 30 s, and operating pressure 5×10^{-1} mBar. During the SEM examination, the accelerating voltage was kept under 5 kV to minimize the beam damage.

In order to investigate the sub-surface damage for a mature process zone at crack tip, the fractured 3PB specimens were selected. The thin sections at the mid-plane that are perpendicular to the fracture surfaces. Prior to microscopic examination, these thin sections were ground and polished by petrographic thinning techniques [35]. The specimen thickness ranged from 80 to 120 μm. The transmitted light optical microscopy (TOM, Olympus, model BH2) was used to obtain the microscopic images, and crossed polars were also used to examine the plastic zone near the pre-crack tip.

3. Results and discussion

3.1. Particle dispersion in HESRNs

The particle dispersion in 80HESRN (III) and 20HESRN (III) is demonstrated in Figs. 1 and 2, respectively. It is noteworthy that this formulation represents the HESRNs with small fraction of NS (3.1 vol%) and high content of CTBN (20.9 vol%). The well dispersed, relatively larger circles shown in the TEM micrographs are regarded as the CTBN particles. In fact, instead of being a constant value, the CTBN particle size can be affected by the CTBN content, types of curing agent and curing conditions [5,36–39]. The diameter of the CTBN particles in Figs. 1 and 2 ranges from 2 to 3 μm, which is compatible with Pearson and Yee's study in the DGEBA/piperidine system [5]. On the other hand, the NS particles form clusters, which distribute between rubber modifiers all over the epoxy matrix in both 80HESRN (III) and 20HESRN (III). These NS clusters are unlike the non-agglomerated NS seen in our previous work in epoxy-silica nanocomposite study [31], which did not possess any CTBN. Under higher magnification, it is unambiguous that the clusters consist of many NS particle (see Fig. 1 (b) and 2 (b)). The NS clustering in HESRNs has not been emphasized yet in the open literature, and the exact reason is not clear. Our speculation would be that at higher CTBN concentrations the COOH groups on one CTBN molecule may attach to two nanosilica particles and forms clustering. Therefore, it is of our interest to evaluate the clustering tendency of NS particles by varying CTBN amount in HESRNs.

Figs. 3 and 4 are the TEM micrographs that show the NS particle dispersion in 80HESRNs (C) and (D) respectively. It is important to note that the formulations in 80HESRNs (C) and (D) represent small fraction of NS (3.1–3.2 vol%) and various CTBN contents (12.0 and 16.6 vol%, respectively). In fact, the NS dispersion shown in Figs. 1–4 indicates NS agglomeration occurs when CTBN content is beyond 12.0 vol%.

3.2. Glass transition temperature

The measured T_gs of the HESRSNs are presented in Table 4. Compared with the CTBN toughened epoxy, the T_gs of the HESRSNs (I–V) mildly decrease due to the addition of NS particles despite the size of NS particles, and the trend of T_g decrease is not proportional to NS content. This observation is somewhat different than the work

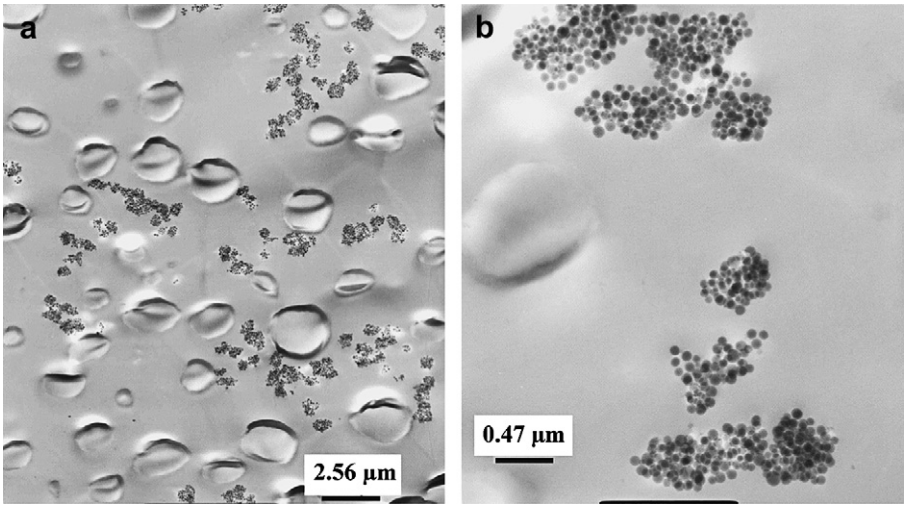

Fig. 1. TEM Micrographs: (a) 80HESRN (III) (b) high-magnification image shows NS clusters.

reported by Kinloch et al. [23], who showed that the addition of NS particles induces a scattering effect on the T_gs of HESRNs within a range of ±6 °C. Generally, the addition of small amount NS particles shows modest effect on the glass transition temperature of HESRNs, while increasing CTBN amount causes T_g drop up to 13 °C.

The T_g reduction due to the addition of CTBN is generally attributed to small amounts of CTBN, which possess a lower T_g, remaining in epoxy matrix after curing [41]. However, the exact reason for the T_g drop due to the presence of NS particles is not clear yet. Theoretically, T_g is strongly related to the level of free volume in polymer matrix and the polymer chain mobility. Several studies have shown that the addition of nanosilica does not significantly increase polymer chain mobility in ESNs [23,31] nor decreases the conversion of the curing reaction between DGEBA and primary or secondary amine groups [40]. Nevertheless, the curing process of epoxy is very complex which involves chemistry and other issues as well. For example, literature has shown that the addition of reactive rubber, CTBN, increases the rate of curing reaction in the amine cured epoxy [39], which strongly affects the mobility of the unreacted curing agent during the curing process. Apparently, more research is needed to interpret the drop of T_g in these HESRNs, and it is beyond the scopes of this study.

3.3. Compressive modulus and compressive yield stress in HESRNs

The compressive moduli of HESRNs (I–V) with fixed CTBN content and HESRNs (A–E) with fixed NS content are plotted in Figs. 5 and 6, respectively. The compressive moduli of HESRNs were obtained from the linear portion of the stress-strain curves in compression tests. Two widely used models, Halpin–Tsai's [41,42] and Kerner's equation [43] are applied to predict the effect of adding rigid fillers and soft particles on the moduli of HESRNs, respectively.

Halpin–Tsai's model is shown in Eq. (2), where E_c, E_m and E_p are Young's modulus of the composite, the matrix, which is taken as 1.62 GPa as the CTBN-modified epoxy, and the NS particles, which is taken as 70 GPa [28], respectively; V_m, V_p is the volume fraction of the polymer matrix and the particle, respectively; ξ is the shape factor of the filler, which equals 2 for spheres.

$$\frac{E_C}{E_m} = \frac{1+\xi\eta V_p}{1-\xi\eta V_p}, \quad \eta = \frac{\frac{E_p}{E_m}-1}{\frac{E_p}{E_m}+\xi} \tag{2}$$

As shown in Fig. 5, the presence of NS particles has a modest effect on the compressive moduli of HESRNs when the NS content is

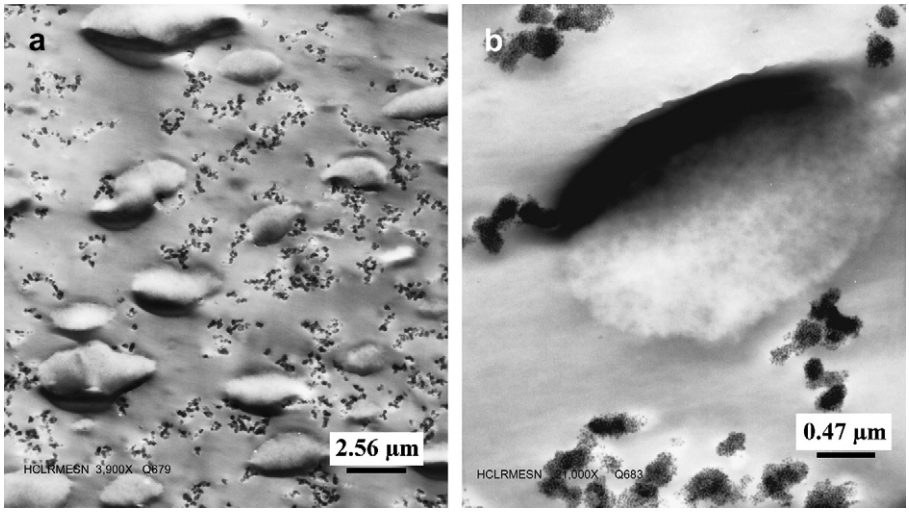

Fig. 2. TEM Micrographs: (a) 20HESRN (III), (b) high-magnification image.

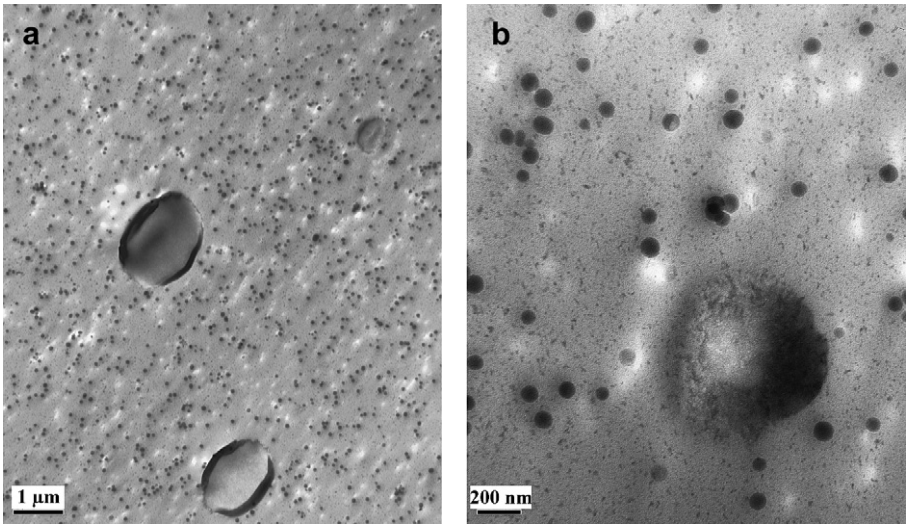

Fig. 3. TEM Micrographs: (a) 80HESRN (C, 12.0 vol% CTBN), (b) high-magnification image.

below 7 vol%. The increase in modulus with NS content for the 80HESRNs agrees well with Halpin–Tsai's model. The moduli of the 20HESRNs are significantly lower than predicted. The low moduli may be due to the lower glass transitions observed for this series. Interestingly, when the NS content is 16.8 vol%, the compressive modulus of HESRNs declines to a level that is lower than the counterparts obtained from the epoxy toughened by CTBN alone. This observation is different than the results in the study of Kinloch and his coworkers [23], which reported that the addition of NS further improves the tensile modulus of the epoxy toughened by 9 wt.% CTBN. Ideally, adding rigid silica spheres into the rubber toughened epoxies can enhance the Young's moduli of the composites. The unexpected drop in compressive moduli is attributed to NS particle clustering, hence the Young's modulus of NS clusters is not equal to the Young's modulus of glass spheres. In fact, a much smaller value of Young's modulus from NS clusters is expected due to the weak internal bonding between NS particles. As a result, the addition of NS particles does not significant improve the compressive moduli of HESRNs in this particular system. The very the same reason can also be used to explain the decline of compressive yield stress of HESRNs (I–V) shown in Table 4.

Kerner's model is shown in Eq. (3), where E_c, E_m, and E_p are the Young's modulus of the composite, the NS toughened epoxy matrix, and the rubber particles, which can be neglected since it is much smaller than the matrix, respectively; V_p, V_m is the volume fraction of the filler particles and matrix, respectively, and ν is the Poisson ratio of matrix.

$$\frac{E_C}{E_m} = \frac{E_m V_m + (\alpha + V_p)E_p}{(1 + \alpha V_p)E_m + \alpha V_m E_p}, \quad \alpha = \frac{2(4 - 5\nu)}{7 - 5\nu} \tag{3}$$

The compressive moduli of HESRNs (A–E) decline when increasing CTBN content. A similar trend of decreasing Young's moduli with increasing the rubber content has been reported in the hybrid composites consisting of micron glass spheres and CTBN [16,17]. It is interesting to note that Kener's model shows somewhat overestimation on the compressive moduli compared to the experimental data. This slight overestimation is attributed to the small amounts of CTBN remaining dissolved in cured epoxy matrix, which has been reported by other investigators [40,41]. The dissolved CTBN in the epoxy matrix increases the polymer chain mobility, which lowers the compressive moduli. In brief, increasing CTBN amount in HESRNs lowers the compressive moduli and yield stress. The

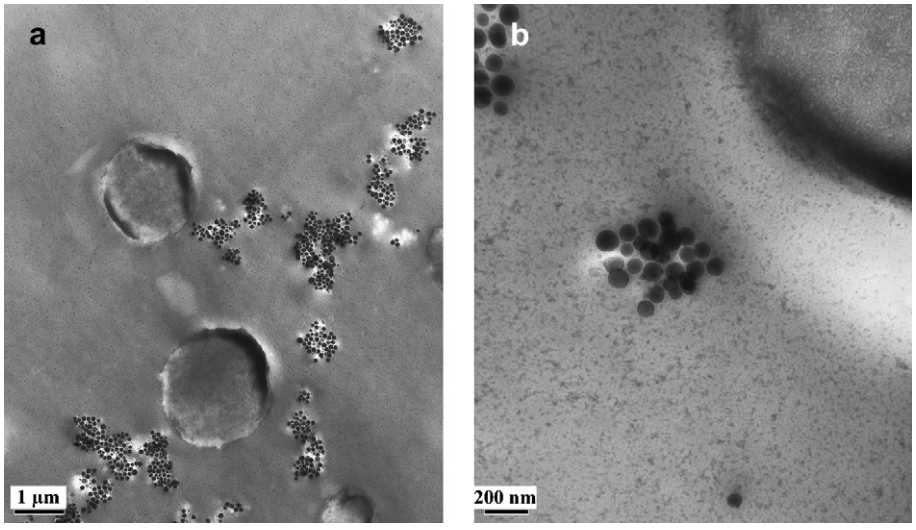

Fig. 4. TEM Micrographs: (a) 80HESRN (D, 16.6 vol% CTBN), (b) high-magnification image demonstrates NS clusters. The noisy background is due to OsO_4 staining.

Table 4
Results of thermal and mechanical tests of HESRNs.

Vol% CTBN	Vol% NS	T_g (°C)		E (GPa)		σ_y(MPa)		K_Q (MPa*m$^{0.5}$)		G_Q (kJ/m^2)	
		80HESRN	20HESRN	80HESRN	20HESRN	80HESRN	20HESRN	80HESRN	20HESRN	80HESRN	20HESRN
20.9	0.0	80.6	80.6	1.62	1.62	55.6	55.6	2.49	2.49	3.25	3.25
20.6	0.8	75.1	70.5	1.64	1.54	59.6	56.8	2.49	2.90	3.21	4.63
20.7	1.5	76.4	71.9	1.37	1.44	57.8	52.8	2.64	2.90	4.31	4.95
20.9	3.1	75.0	70.0	1.66	1.37	57.4	52.8	2.67	3.04	3.64	5.72
21.3	6.4	72.7	71.1	1.78	1.47	54.9	52.1	2.08	2.80	2.06	4.52
22.6	16.8	72.8	75.4	0.85	1.37	25.9	38.0	1.48	1.84	2.18	2.10
0.0	3.2	88.2	80.7	2.69	2.46	94.9	88.5	1.67	1.84	0.88	1.17
3.7	3.2	75.6	78.7	1.76	1.77	72.5	73.9	2.85	2.76	3.91	3.65
6.0	3.2	78.1	78.7	2.04	2.08	86.0	85.6	2.91	2.81	3.52	3.22
12.0	3.2	80.8	75.5	1.80	1.74	76.6	73.3	3.22	3.43	4.88	5.73
16.6	3.1	79.9	76.4	1.54	1.52	63.8	62.7	3.23	3.15	5.74	5.54
20.9	3.1	75.4	72.8	1.72	1.50	59.4	53.7	2.67	3.04	3.64	5.72

addition of small amounts of NS particles has a negligible influence on compressive moduli and yield stress, when comparing the experimental data of HESRNs and epoxy-rubber blends (ERBs) under the same amount of CTBN.

3.4. Fracture behavior in HESRNs

It is important to note that the conditional fracture toughness, K_Q, which is calculated by the P_Q load, is used here. According to ASTM 5045 guidelines, P_Q is determined by the intersection point of load-displacement curve and the drawn intersection line. The compliance of the drawn intersection line equals to 105% multiplies the initial compliance of the linear portion of the load-displacement curve. The ratio of P_{max}/P_Q should be less than 1.1 to obtain the valid K_Q [33].

Fig. 7 contains the fracture toughness of HESRNs (I–V) versus NS content. Both 20HESRNs and 80HESRNs exhibits maximum K_Q peaks when NS content is low, but K_Q values decrease to a level even lower than the epoxy toughened by CTBN alone when NS content is 16.8 vol%. The improvement of fracture toughness in HESRNs due to the presence of small amounts of NS particles is not as much as that in epoxy-silica nanocomposites (ESNs). In addition, the 20HESRNs generally demonstrates higher K_Q values than 80HESRNs in each composition.

As shown in Fig. 8, the improvement of fracture energy of HESRN is considerable. For example, the G_Q value in 20HESRN (III) is almost 1.5 folds of the counterpart in the epoxy toughened by CTBN alone. Although a different toughening behavior of the HESRNs can be found in the literature [23], our observation is in agreement with the study reported by Sprenger et al. [21,22]. It indicates the DGEBA/piperidine lightly crosslinked system is more comparable with the case of using room temperature cured, ATBN (amine terminated butadiene nitrile polymer) modified epoxy concerning the toughening properties.

The fracture toughness of HESRNs (A–E) is plotted versus CTBN content in Fig. 9. Compared to ERBs (shown as the bottom curve by dot line), it is clear that the addition of small amount of NS can further enhance the fracture toughness to a level beyond 3.0 MPa*m$^{0.5}$, which is not able to be achieved by increasing CTBN content alone. Compared to ERBs/CTBN, the K_Q improvement owing to the addition of NS particles exhibits an additive effect, which roughly equals to 0.7 MPa*m$^{0.5}$ until the CTBN content is beyond 12.0 vol%. The K_Q value seen here is very close to the K_{IC} obtained from the neat epoxy resin and ESNs (see Fig. 7). However, the additive improvement of fracture toughness in HESRNs (A–E) diminishes at the high CTBN content region (16.6–20.9 vol%), where the TEM images have shown NS clustering (see Figs. 1–4). It reveals the NS agglomeration has a negative effect on the fracture toughness improvement of HESRNs. Additionally, the 20HESRNs and 80HESRNs possess the same magnitude K_Q values when data scattering is considered, i.e. no NS particle size effect on fracture toughness is observed in HESRNs (A–E). The superior toughening behavior in 20HESRNs shown in Figs. 7 and 8 is considered as atypical case since it is only presented in high CTBN content region with NS agglomeration.

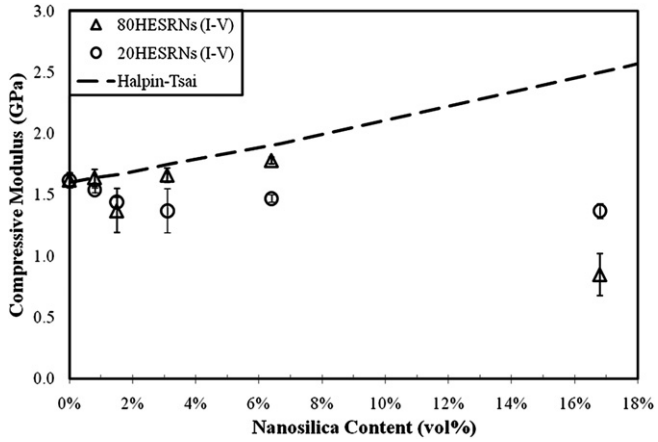

Fig. 5. Compressive moduli of HESRNs (I–V) versus NS content (CTBN content is 18 wt.%).

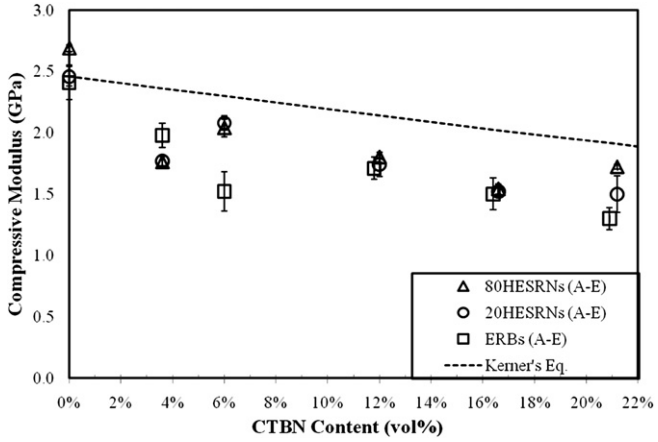

Fig. 6. Compressive moduli of HESRNs (A–E) versus CTBN content (NS content is 5 wt.%).

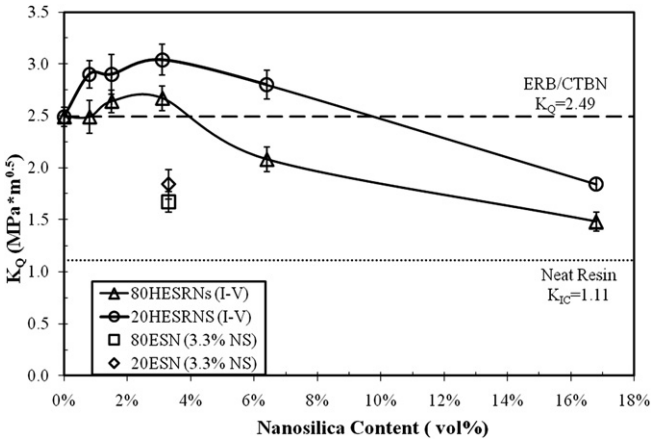

Fig. 7. Fracture Toughness of HESRNs (I–V) versus NS content (CTBN content is 18 wt.%).

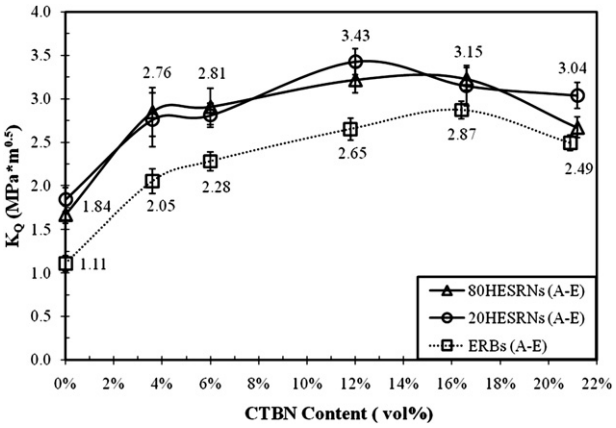

Fig. 9. Fracture Toughness of HESRNs (A–E) vs. CTBN content (NS content is 5 wt.%).

3.5. Fracture surface in HESRNs

The fracture surface investigations here focus on the beginning of the stress whitening zone, which is located after the pre-crack region. The stress whitening, which mainly results from the light scattering due to rubber particle cavitation and matrix dilation, is essential to the energy absorbing mechanism [5]. Fig. 10 is a series of micrographs taken from the fractured SEN-3PB specimen of 80HESRN (III) with 3.1 vol% NS and 20.9 vol% CTBN. The dark circles shown in micrographs are considered as rubber particle cavitation and consequent matrix dilation since its' recess nature scatters more electrons. NS clustering, which can be clearly observed within the matrix between rubber particle cavitation in Fig. 10 (b), shows a size within submicron to micron range and corroborates the observations from the TEM micrographs. Similar fractographic morphology is also shown in 20HESRN (III) under SEM (pictures not shown).

Johnsen et al. [28] have shown that the size of NS is too small to pin the crack opening displacement (COD), when NS particles are well dispersed in epoxy matrix. This argument is accepted by other researchers in toughening mechanism studies of rigid nano particles filled epoxies [29,31]. However, according to our previous calculation [31], the COD in this neat epoxy system is 4.7 μm, which is on a similar scale of NS agglomerations. As a result, crack pinning model should not be excluded from the consideration of toughening mechanisms when NS particles agglomerate. It is important to bear in mind that the toughening effect of using NS clusters is expected to be less than the micron-size silica particles toughened counterparts because of the weak internal bonding between NS particles inside the agglomerations. It is worthy to mention that several attempts were made to obtain the evidence of well dispersed NS particle debonding in HESRNs. However, it is difficult

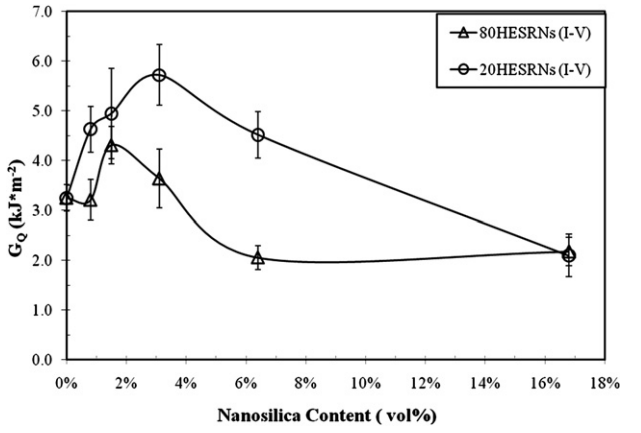

Fig. 8. Fracture Energy of HESRNs (I–V) versus NS content (CTBN content is 18 wt.%).

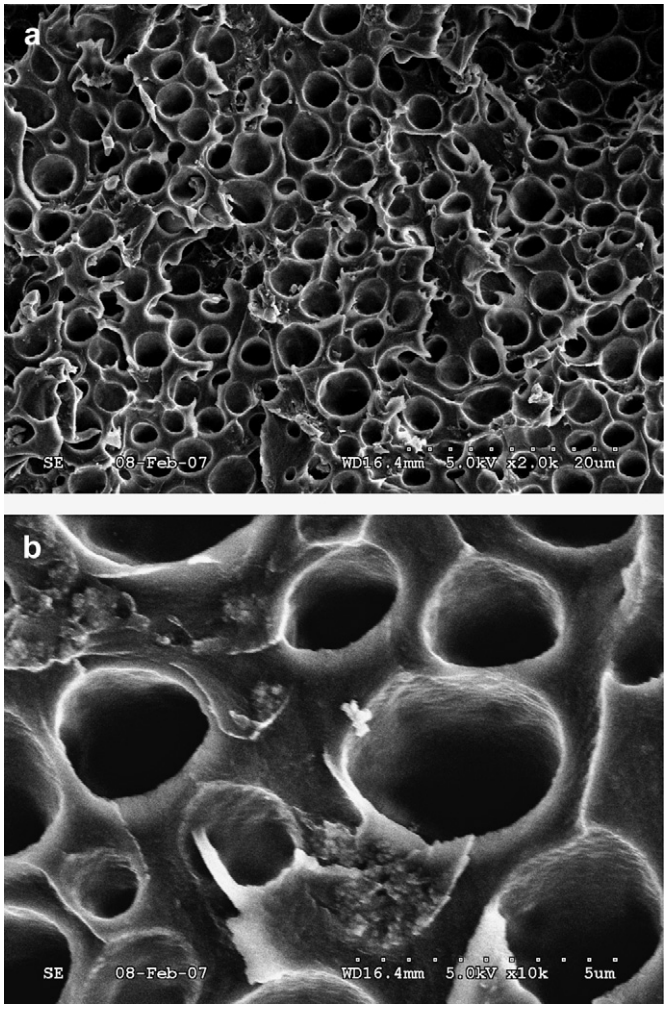

Fig. 10. Fracture surface images of 80HESRN (III): (a) rubber cavitation inducing massive matrix dilation, and (b) 80NS agglomeration. Note the crack growth direction is from the bottom toward the top.

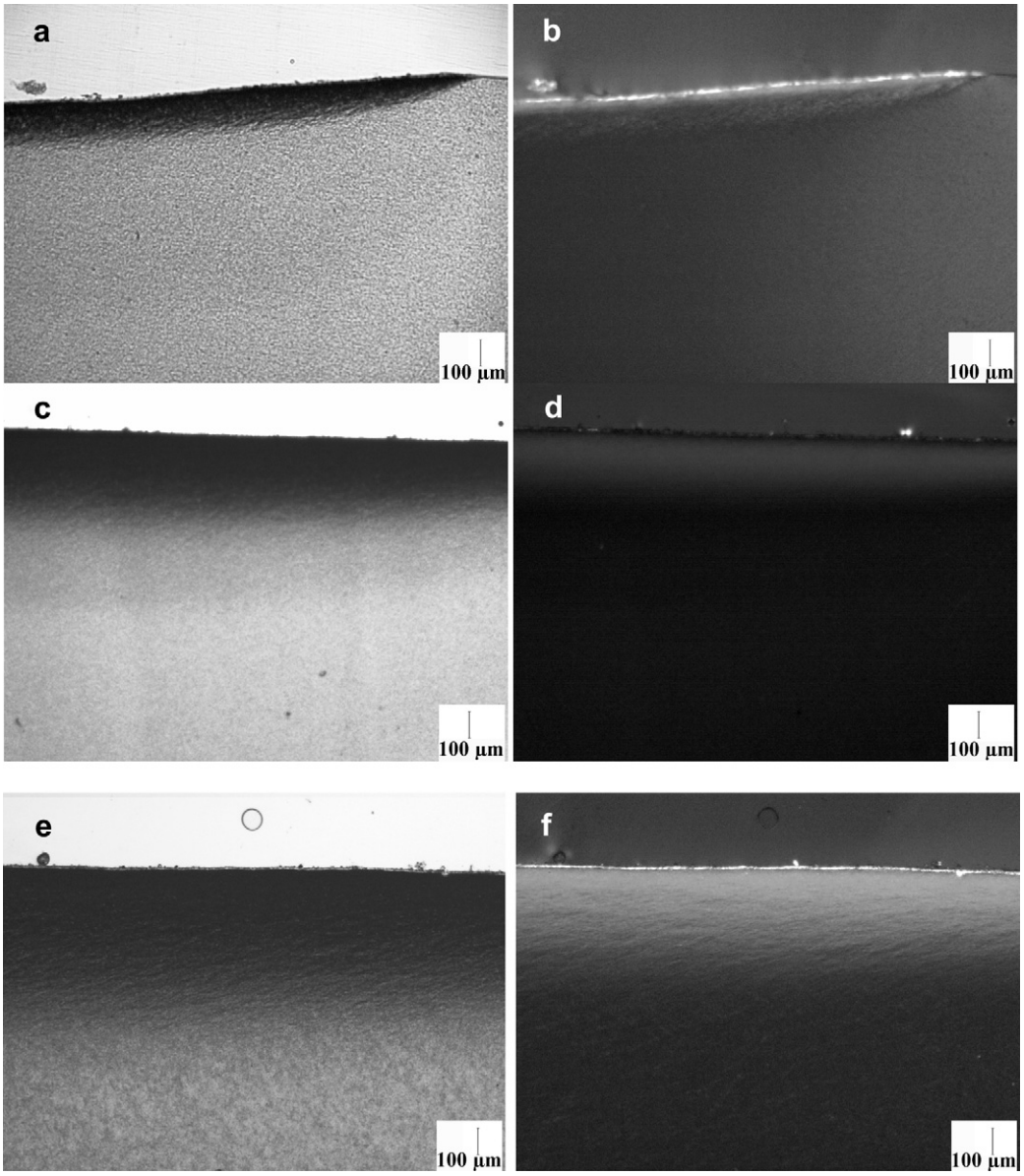

Fig. 11. TOM micrographs: (a) 80HESRN (B, 2.91 MPa*m$^{0.5}$) under bright field, (b) under cross polars, (c) 80HESRN (C, 3.22 MPa*m$^{0.5}$) under bright field, and (d) under cross polars, (e) 80HESRN (D, 3.23 MPa*m$^{0.5}$) under bright field, and (f) under cross polars.

to provide high resolution images in such small scale at this stage due to the rough surface caused by rubber cavitation. More investigations are needed to elucidate the interaction between CTBN rubber and NS particles in HESRNs.

3.6. Subsurface damage in HESRNs

Figs. 11 and 12 are series of TOM micrographs taken under bright filed or crossed polars for the 80HESRNs (B∼D), and ERBs/CTBN (BD) respectively. The crack growth direction in the TOM micrographs is from the right to the left. Note that the magnification in Fig. 11 is twofold as the one in Fig. 12. In bright field, both HESRNs and ERBs show light scattering dark bands, which are considered to be caused by rubber particle cavitation and matrix dilation when crack slowly propagates throughout the specimen. On the other hand, the same regions also show bright birefringence under cross polars, which indicates the massive matrix shear yielding occurred.

As shown in Figs. 11 and 12, the size of plastic zone (depth of the band) increases not only when increasing the amount of CTBN, but also when blending small amount of NS particles into ERBs. In order to demonstrate the relationship between plastic zone size, fracture toughness and yield stress, Irwin's model [44] and the plastic zone size measured from 20HESRNs, 80HESRNs and ERBs are plotted in Fig. 13.

In Irwin's model (shown in Eq. (4)), the K_{IC} is the critical stress intensity factor, and it is assumed that K_Q equals K_{IC} in this estimation; σ_y is the tensile yield stress, which can be estimated as the compressive yield stress multiplied by 0.7 according to ASTM 5045 [32], and r_p is the radius of the plastic zone, which is measured as the width of the bands seen in TOM images. Each r_p presented in Fig. 13 uses the average of two measured values: one is the band width obtained under bright field, and the other one is the counterpart measured under crossed polars. The error bars in Fig. 13 indicate the difference between those two measured widths.

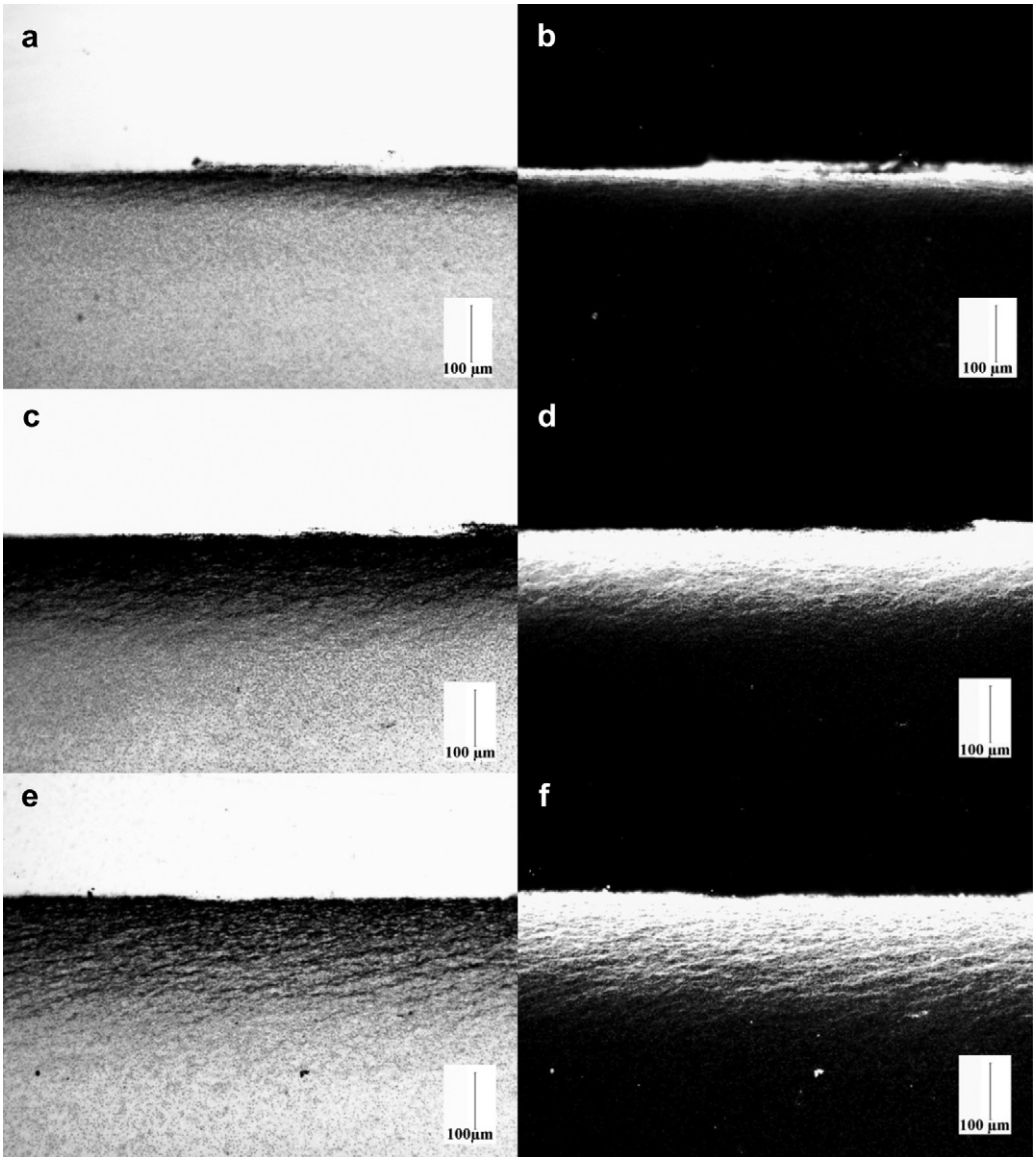

Fig. 12. TOM micrographs: (a) ERB(B, 2.28 MPa*m$^{0.5}$) under bright field, (b) under cross polars, (c) ERB(C, 2.65 MPa*m$^{0.5}$) under bright field, (d) under cross polars, (e) ERB(D, 2.87 MPa*m$^{0.5}$) under bright field, and (f) under cross polars. Note the magnification used in this figure is larger than that in Fig. 11.

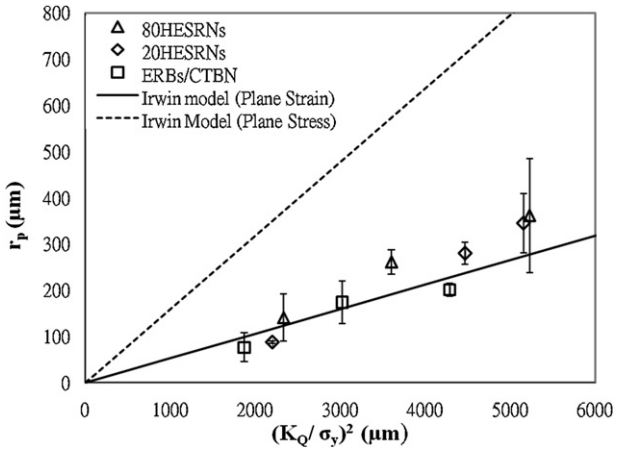

Fig. 13. Measured plastic zone size of HESRNs and ERBs vs. $(K_{IC}/\sigma_y)^2$.

$$r_p = \frac{K_{IC}^2}{(6\pi)\sigma_y^2} \text{for plane strain}, \quad r_p = \frac{K_{IC}^2}{(2\pi)\sigma_y^2} \text{for plane stress} \tag{4}$$

The measured r_p values from HESRNs and ERBs are scattered and located in a region whose upper and lower limits can be described from Irwin's model under plane-stress stress state and plane-strain stress state, respectively. Such observation suggests there is a stress state transition. According to ASTM 5045 guidelines, the plane-strain criterion can be quantitatively specified as following: the thickness of the 3PB specimens, which is 6.4 mm in this study, should be larger than the value of $2.5*(K_{IC}/\sigma_y)^2$. Table 5 contains the experimental and calculation results in regard to the plane-strain criterion. It is clear that the addition of large amount CTBN (more than 12 vol%) significantly lowers the yield stress. Therefore, the stress state may transform from pure plane-strain to partial plane-strain and consequently cause more variables for data interpretation.

3.7. Toughening mechanisms in HESRNs

Understanding the toughening mechanisms in HESRNs is never an easy task. At least two difficulties have to be overcome: the complex due to their multi-component nature, and the multi-scale phenomena range from macroscopic to microscopic at nanometer scale. Although the toughening mechanisms of HESRNs are not completely understood yet at this stage, a reasonable hypothesis can be proposed based on the wisdom collecting from literature and on aforementioned experimental observations.

From literature, one may conclude that the toughening mechanisms caused by rubber particles and NS particles are somewhat similar. For rubber particles, it is well accepted that, rubber cavitation induced shear banding and matrix dilation (or plastic void growth) reduce the effective crack opening force by developing a plastic zone, which shields the crack tip. As a result, the size of the plastic zone is generally proportional to the square of toughness of the giving system [6,45]. For NS particles, Johnsen et al. [28] first demonstrated the importance of matrix dilation in toughening mechanisms of ESNs. Zhang et al. showed that the addition of NS particles into neat epoxy matrix introduces more local plastic deformation near the crack tip, and has recognized its importance in toughening behavior [46]. Recently, our previous study in a lightly crosslinked epoxy matrix verified the plastic deformation and further pointed out that it consists of shear yielding and matrix dilation [31].

From this presented study, it appears that toughening mechanisms for rubber particles and NS particles remain the same when combined in HESRNs. The SEM images show rubber cavitation plus local matrix dilation on fracture surface. The bright birefringence under cross polars reveals the massive matrix shear yielding. More importantly, blending small amount of NS particles into ERBs further enlarge the plastic zone, which can blunt the crack propagation.

The question raised here is that if the toughening mechanisms of rubber particles and NS particles are similar, why adding NS particles into ERBs can further enhance the fracture toughness to a level which is not able to be achieved by using CTBN alone? At this stage, the authors tend to attribute this toughening effect to the substantial difference in interparticle distance between the micron-size CTBN rubber particles and the nanometer size NS particles used in the presented study for following reasons.

Many studies reported that adding small amount of rigid nanofiller into polymer matrix enhances the fracture toughness when the filler is well exfoliated [27–31]. The performance shows certain levels of particle size dependence which is more substantial when the filler size shrinks from micron to nanometer scale [47]. One of the many explanations is that nanometer size filler is more efficient to trigger toughening mechanisms, compared with micron-size counterpart, since more polymer matrix is in the vicinity of toughening agents, where the stress state is altered. In a spherical silica toughened epoxy system, Adachi et al. [47] focused on the effects of particle size, which ranges from micron to nanometer scale, and volume fraction on fracture toughness. They suggested that the enhanced fracture toughness (ΔK_{IC}) is proportional to the reciprocal of the square root of the interparticle distance (surface to surface). Although predicting the fracture toughness of HESRNs by Adachi's model is not appropriate because of the complex nature of the system presented here, using the interparticle distance concept is still beneficial to the interpretation. The interparticle distance (surface to surface), τ, which is shown in Equation (5) for a cubic distribution, ideal dispersion scenario, is able to dramatically decrease due to the decrease of particle size. For example, when 12 vol% CTBN rubber particle with nominal 3 μm is used, τ is approximately 1.9 μm, which implies that there is certain amount of intact polymer matrix for nanofiller, such as 20NS or 80NS particles, to trigger more shear yielding and matrix dilation. This explanation is further supported by our preliminary studies in another HESRN system consisting of nanometer size core-shell rubber particles and 20NS particles [48]. More specifically speaking, 10 vol% CS rubber particles with nominal 50 nm diameter were used to replace CTBN, and the rest of the material preparation is the same as the aforementioned 20HESRNs. The interparticle distance between CS rubber particles roughly decreases to 37 nm, which is in the similar scale to 20NS particles. As a result, is it not surprising that blending various amounts of 20NS particles (0.8–6.4 vol%) in the HESRNs with CS particles do not further increase the fracture toughness.

$$\tau = d\left[\left(\frac{\pi}{6\Phi_p}\right)^{\frac{1}{3}} - 1\right] \tag{5}$$

where Φ_p is the particle volume fraction, and d is the particle diameter.

Table 5
The results of K_Q, σ_y, and values of $2.5*(K_Q/\sigma_y)^2$.

	K_Q (MPa*m$^{0.5}$)	Compressive yield stress (MPa)	r_p (μm)	$2.5*(K_Q/\sigma_y)^2$ (mm)
80HESRN (B, 6% CTBN)	2.91	86.0	141	5.8
80HESRN (C, 12% CTBN)	3.22	76.6	268	9.0
80HESRN (D, 16% CTBN)	3.23	63.8	380	13.1
20HESRN (B, 6% CTBN)	2.81	85.6	88	5.5
20HESRN (C, 12% CTBN)	3.43	73.3	280	11.1
20HESRN (D, 16% CTBN)	3.15	62.7	346	12.9
ERB/CTBN (B, 6% CTBN)	2.28	75.3	77	4.7
ERB/CTBN (C, 12% CTBN)	2.65	68.8	175	7.6
ERB/CTBN (D, 16% CTBN)	2.87	62.6	193	10.7

4. Summary

In order to study the toughening mechanisms in hybrid epoxy-silica-rubber nanocomposites (HESRNs), two different size nanosilica (NS) particles (20 nm and 80 nm in diameter), were individually blended into CTBN toughened, DGEBA/piperidine epoxies. The addition of NS results in a minor decline of the T_gs for the HESRNs. It is interesting that NS particle clustering occurs when high amount of CTBN is used. Both compressive moduli and yield stress are not significantly increased when NS particles are added but do decline with increasing CTBN content. The toughening effect of adding NS particle is significant. The fracture toughness of HESRNs is further improved to a level which is not able to be achieved by increasing CTBN amount alone. The increase in fracture toughness with NS particle addition to CTBN-modified epoxies appears to be an additive effect and is diminished when the NS particles cluster. Moreover, the particle size effect of NS particle on toughening behavior is not considerable except the case which NS clustering is observed.

The toughening mechanisms in ERBs were found to be rubber particle cavitation that induced plastic matrix deformation consisting of matrix dilation and matrix shear banding. Such results agree with the large body of literature on rubber toughened epoxies. The addition of NS to rubber toughened epoxy results in HESRNs. The NS enhances the plastic deformation in the process zone that enlarges the zone size in front of the crack tip. We speculate that this enhancement involves an increase in shear band density between rubber particles in the plastic zone. The expanded plastic zone further shields the crack tip and therefore improves the fracture toughness. Irwin's model provides a reasonable prediction

for the relationship between plastic zone size and fracture toughness in both ERBs and HESRNs.

Acknowledgments

The authors would like to thank 3M, Dow Chemical Company, Emerald Performance Materials, and Nanoresins for providing the materials free of charge, and the financial support from the Lehigh University/Mid-Atlantic Partnership, NASA Nanomaterials (NASA coop agreement No. NNX06AD01A), and the Semiconductor Research Corporation (SRC). Acknowledgments toward Dr. Gregory Hendricks at Core Electron Microscopy Facility, UMass Medical School for the TEM micrographs.

References

[1] Kinloch AJ, Shaw SJ, Tod DA, Hunston DL. Polymer 1983;24:1341–54.
[2] Huang Y, Kinloch AJ. J Mater Sci 1992;27:2753–62.
[3] Huang Y, Kinloch AJ. J Mater Sci 1992;27:2763–9.
[4] Yee AF, Pearson RA. J Mater Sci 1986;21:2462–74.
[5] Pearson RA, Yee AF. J Mater Sci 1986;21:2475–88.
[6] Pearson RA, Yee AF. J Mater Sci 1991;26:3828–44.
[7] Lange FF. Phil Mag 1971;22:983–92.
[8] Rose LRF. Mech Mater 1987;6:11–5.
[9] Faber KT, Evans AG. Acta Metall 1983;31(4):565–77.
[10] Faber KT, Evans AG. Acta Metall 1983;31(4):577–84.
[11] Evans AG, Williams S, Beaumont PWR. J Mater Sci 1985;20:3668–72.
[12] Lee J, Yee AF. Polymer 2001;42:577–88.
[13] Lee J, Yee AF. Polymer 2001;42:589–97.
[14] Pearson RA, Yee AF. J Appl Polym Sci 1993;48:1051–60.
[15] Kinloch AJ, Maxwell DL, Young RJ. J Mater Sci 1985;20:4169–84.
[16] Maazouz A, Sautereau H, Gerard JF. J Appl Polym Sci 1993;50:615–26.
[17] Zhang H, Berglund LA. Polym Eng Sci 1993;33(2):100–7.
[18] Lee J, Yee AF. Polym Eng Sci 2000;40(12):2457–70.
[19] Azimi HR, Pearson RA, Hertzberg R. J Appl Polym Sci 1995;58:449–63.
[20] Azimi HR, Pearson RA, Hertzberg R. Polym Eng Sci 1996;36:2352–65.
[21] Kinloch AJ, Lee JH, Taylor AC, Sprenger S, Eger C, Egan D. J Adhes 2003;79:867–73.
[22] Sprenger S, Eger C, Kinloch AJ, Lee JH, Taylor AC, Egan D. Spec Issue adhesion KLEBEN DICHTEN 2004;3.
[23] Kinloch AJ, Mohammed RD, Taylor AC, Eger C, Sprenger S, Egan D. J Mater Sci 2005;40:5083–6.
[24] Sprenger S, Kinloch AJ, Taylor AC, Mohammed RD, Eger C. JEC Composites 2005;19:73–5.
[25] Sprenger S, Kinloch AJ, Taylor AC, Mohammed RD. JEC Composites 2005;21:66–9.
[26] Sprenger S, Kinloch AJ, Taylor AC, Mohammed RD. JEC Composites 2007;30:54–7.
[27] Zhang H, Zhang Z, Friedrich K, Eger C. Acta Materialia 2006;54:1833–42.
[28] Johnsen BB, Kinloch AJ, Mohammed RD, Taylor AC, Sprenger S. Polymer 2007;48:530–41.
[29] Zhao S, Schadler LS, Duncan R, Hillborg H, Auletta T. Compos Sci Technol 2008;68(14):2965–75.
[30] Watzel B, Rosso P, Haupert F, Friedrich K. Engng Fract Mechan 2006;73:2375–98.
[31] Liang YL, Pearson RA. Polymer 2009;50:4895–905.
[32] ASTM 1996;76(D695–D696):76–82.
[33] ASTM 1999;800(D5045–D5099):800–8.
[34] Pearson RA. Ph. D. dissertation. Ann Arbor, MI: Michigan University; 1990 [chapter 2].
[35] Holik AS, Kambour RP, Hobbs SY, Fink DG. Microstruct Sci 1979;7:357–67.
[36] Pearson RA, Yee AF. J Mater Sci 1989;24:2571–80.
[37] Kinloch AJ, Hunston DL. J Mater Sci Lett 1986;5:909–11.
[38] Russell B, Chartoff R. Polymer 2005;46:785–98.
[39] Wise CW, Cook WD, Goodwin AA. Polymer 2000;41:4625–33.
[40] Ghaemy M, Amini SM, Barghamadi M. J Appl Polym Sci 2007;104:3855–63.
[41] Halpin JC, Tsai SW. Enviromental factors in composite materials design. In: AFML-TR67–423. Air Force Materials Laboratory; 1969.
[42] Halpin JC, Kardos JL. Polym Eng Sci 1976;16:344–52.
[43] Kerner EH. Proc Phys Soc 1956;69B:808–13.
[44] Irwin GR. In: Proceedings of the seventh sagamore conference. Syracuse NY: Syracuse University; 1960, (vol. II, 63).
[45] Ritichie RO. Mat Sci Eng 1987;A103:15–28.
[46] Zhang H, Tang LC, Zhang Z, Friedrich K, Sprenger S. Polymer 2008;49:3816–25.
[47] Adachi T, Osaki M, Araki W, Kwon SC. Acta Materialia 2008;56:2101–9.
[48] Liang YL. Ph. D. dissertation: Lehigh University; 2009.